Palladium Oxide Nanoparticles: Preparation, Characterization and Catalytic Activity Evaluation

Maurizio Muniz-Miranda [1,2,*] , **Angela Zoppi [2]** , **Francesco Muniz-Miranda [3]** and **Nicola Calisi [4,5]**

[1] Department of Chemistry "Ugo Schiff", Via Lastruccia 3, 50019 Sesto Fiorentino, Italy
[2] Institute of Complex Systems (CNR), Via Madonna del Piano 10, 50019 Sesto Fiorentino, Italy; angeppi@libero.it
[3] Chimie ParisTech, PSL Research University, CNRS, Institute of Chemistry for Life and Health Sciences, F-75005 Paris, France; f.muniz-miranda@chimieparistech.psl.eu
[4] Department of Industrial Engineering, Via di Santa Marta 3, 50139 Firenze, Italy; nicola.calisi@unifi.it
[5] National Interuniversity Consortium of Materials Science and Technology, INSTM, Via G. Giusti 9, 50121 Firenze, Italy
* Correspondence: maurizio.muniz@unifi.it

check for updates

Abstract: Stable palladium oxide nanoparticles were prepared in aqueous suspension with a very simple procedure, by dissolving palladium nitrate in water at a concentration around 10^{-4} M. UV-visible absorption spectroscopy was adopted to follow the formation of these nanoparticles, which were characterized by TEM microscopy, along with XRD, XPS and Raman measurements. DFT calculations allowed to interpret the Raman data and to clarify the species present at the surface of the nanoparticles. The catalytic activity of the latter was evaluated by monitoring the reduction of *p*-nitrophenol to *p*-aminophenol. This investigation paves the way to the use of these colloidal nanoparticles in processes of heterogeneous catalysis, in particular those concerning the catalytic degradation of aromatic derivatives that represent a serious danger for the environment as pollutants, as in the case of *p*-nitrophenol.

Keywords: palladium oxide; nanoparticles; XRD; spectroscopic characterization; DFT

1. Introduction

Due to the optimal combination of activity and selectivity, palladium is one of the most used transition metals for both homogeneous and heterogeneous catalysis of organic reactions [1,2]. In general, heterogeneous catalytic processes are preferred with respect to homogeneous ones due to the higher yields and easier reusability of the catalytic material. Since heterogeneous catalysis is based on processes taking place at the surface, the use of finely dispersed catalysts is often adopted in order to reduce the amount of material and maximize its catalytic effect [3,4]. For this purpose, palladium nanoparticles are widely used to catalyze organic reactions [5–14]. Similar to palladium, palladium(II) oxide (PdO) has also found applications in many catalytic processes [15–18], but few studies were carried out on the production of palladium oxide nanoparticles compared to the wide range of works concerning metallic palladium particles [19–22]. A problem in obtaining colloidal suspension of PdO nanoparticles derives from the agglomeration of them, so it was often necessary to introduce surfactants or supporting materials that favored their stability. In this work, we propose a simple method to obtain stable palladium oxide nanoparticles dispersed in water, without the need of additives. The characteristics of the nanoparticles have been investigated by different techniques and their catalytic activity has been evaluated by monitoring the reduction reaction of *p*-nitrophenol to *p*-aminophenol.

2. Materials and Methods

2.1. Materials

Palladium(II) nitrate ($Pd(NO_3)_2$, purity 95%) was furnished by BOC Sciences (Shirley, New York, USA), *p*-nitrophenol (PNP, purity ≥ 99%) and sodium borohydride ($NaBH_4$, purity 98%) by Sigma-Aldrich (St. Louis, Missouri). Insoluble palladium oxide is spontaneously formed by the dissolution of palladium nitrate in water, in the form of extremely small nanoparticles, as shown in detail in the Results Section. A portion of the colloidal suspension was used to perform absorption, ζ-potential and microscopy measurements, and another portion was ultra-centrifuged to obtain a dark precipitate, which was rinsed in pure water for X-Ray diffraction (XRD), X-ray Photoelectron Spectroscopy (XPS) and Raman investigation.

2.2. ζ-Potential

Analysis was performed with a Zetasizer Nano ZS90, Malvern Instruments (Malvern, UK).

2.3. Microscopy

Transmission electron microscopy (TEM,) measurements were obtained by using a Philips EM 201 instrument (Philips Electronic Instruments, Amsterdam, The Netherlands) with an electron beam emitted at 80 kV, after placing a drop of colloidal sample on a carbon–Cu grid.

2.4. Absorption

UV–visible absorption spectra were obtained in the 200–800 nm region by using a Cary 5 spectrophotometer (Varian, Palo Alto, CA, USA).

2.5. X-ray Diffraction

X-ray diffraction (XRD) was performed in a Bruker model D8 Advance diffractometer (Billerica, MA, USA) after drop casting the centrifuged colloidal solution of PdO nanoparticles on a silicon substrate. Data were presented after background subtraction. Resulting diffraction patterns were analyzed with the dedicated DIFFRAC.EVA (Bruker, Version 3.0). Software automatically compared the experimental data with the reference database, where the Power Diffraction Files (PDF)s are relative to palladium oxide and palladium nitrate, PDF 85-0624 and PDF 01-0398, respectively.

2.6. X-ray Photoelectron Spectroscopy

XPS measurements were performed using a non-monochromatic Mg Kα x-ray source (1253.6 eV) and a VSW HAC 5000 hemispherical electron energy analyzer operating in the constant-pass-energy mode at E_{pas} = 44 eV. The samples were prepared by dropping the centrifuged colloidal suspension on soda-lime glass substrates. After drying, they were introduced in the ultra-high vacuum (UHV) system via a loadlock under inert gas (N_2) flux and kept in the introduction chamber overnight, allowing the removal of volatile substances, as confirmed by the achieved pressure value (2×10^{-9} mbar), just above the instrument base pressure. The obtained spectra were referenced to C 1s core peak at 284.8 eV assigned to the adventitious carbon. The spectra were fitted using CasaXPS (software version 2.3.15) after removal of a Shirley-type background.

2.7. Raman Scattering

Raman spectra of the bimetallic nanoparticles deposited on an aluminum plate were measured in different points of the dried sample by using a Renishaw RM2000 micro-Raman instrument (Renishaw, Wotton-under-Edge, UK), equipped with a diode laser emitting at 785 nm. Sample irradiation was accomplished by using the 50x microscope objective of a Leica Microscope DMLM (Leica Microsystems, Wetzlar, Germany). The backscattered Raman signal was fed into the monochromator through 40 μm

slits and detected by an air-cooled CCD (2.5 cm^{-1} per pixel), filtered by a double holographic Notch filters system. Spectra were calibrated with respect to a silicon wafer at 520 cm^{-1}.

2.8. Density Functional Theory (DFT) Calculations

Density Functional Theory (DFT) calculations were carried out using the GAUSSIAN 09 package [23]. Optimized geometries were obtained at the DFT level of theory, employing the widely adopted Becke 3-parameter hybrid exchange functional (B3) combined with the Lee–Yang–Parr correlation functional (LYP) [24,25], along with the Lanl2DZ basis set and pseudopotential [26–28]. The latter was successfully used in the simulation of the Raman spectra of complexes containing heavy metals [29–31]. All parameters were let free to relax and all calculations converged toward optimized geometries corresponding to energy minima, as revealed by the lack of negative values in the frequency calculation. A scaling factor of 0.98 for the calculated harmonic wavenumbers was employed, as usually performed in calculations at this level of theory [32–36].

2.9. Catalysis Tests

NaBH$_4$ was added to the aqueous solution of PNP (PNP concentration: 7 µM; NaBH$_4$ concentration: 3.6 mM). The NaBH$_4$/PNP concentration ratio was about 500. The resulting solution was stirred for 30 s and observed by UV-vis absorption measurements for 30 min. Then, after adding a small amount of the PdO colloid (Pd concentration: 5 µM), the same absorption measurements were performed.

3. Results

We have noted that, after dissolving Pd(NO$_3$)$_2$ in small amount (around 2×10^{-4} M concentration) in water at room temperature, the aqueous solution progressively turned toward a marked yellowish color. This evidence can be monitored by the UV-visible absorption spectrum, where a band grows around 265 nm, with a pronounced tail in the visible region (Figure 1). However, after five hours from the dissolution, no further changes in the absorption spectrum were detectable. The final pH of the solution was ~4. The UV-visible absorption band around 265 nm can be confidently attributed to highly dispersed palladium oxide [37,38]. Actually, the existence of nanoparticles in aqueous suspension has also been demonstrated by TEM microscopy, after depositing drops of solution on a carbon-Cu grid (see Figure 2).
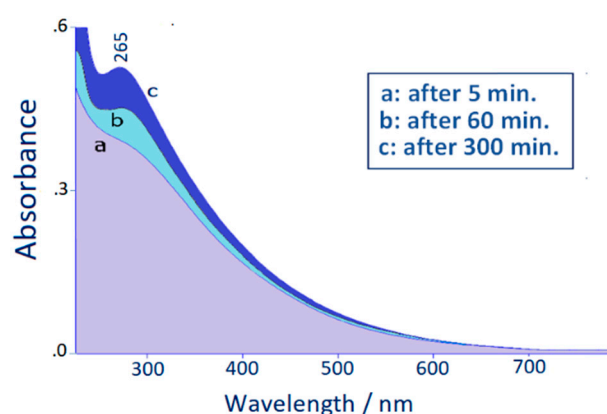

Figure 1. UV-vis absorption spectra of the aqueous sample of palladium nitrate, after different times from the dissolution (optical path length (OPL) = 1 cm).

The TEM micrograph shows small nanoparticles (average diameter: 2.2 nm), which are mostly monodispersed and quite similar in their shapes and dimensions. The zeta potential measurements validate the stability of the colloidal dispersion, showing a peak at +35 mV.
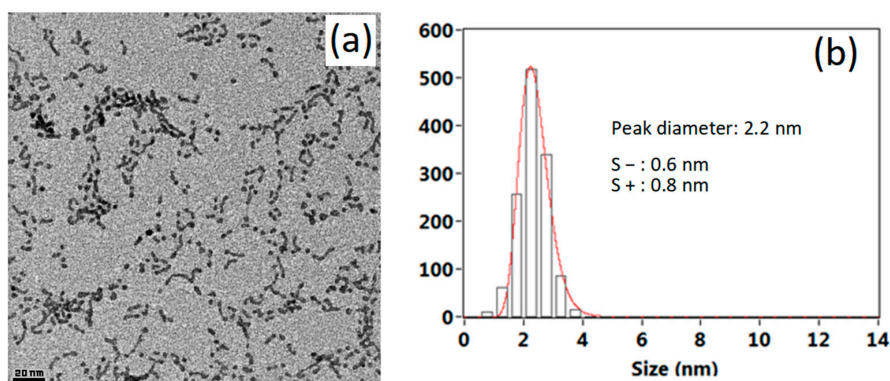
Figure 2. (**a**) Transmission electron microscopy (TEM) micrograph of the aqueous sample of palladium nitrate, after deposition on carbon-Cu grid, and (**b**) particle size distribution.

A mechanism of formation of the palladium oxide nanoparticles can be proposed (Scheme 1). When $Pd(NO_3)_2$ is dissolved in aqueous solution, insoluble PdO is spontaneously produced in the water environment as small nanoparticles. The first step is the hydration of the palladium cation with the formation of Pd(II) tetrahydrate [39–41]. This aquacomplex, through the formation of palladium hydroxide, can give rise to PdO, which is the stoichiometry corresponding to the most stable form of palladium oxide.

$$Pd^{+2} + 4\ H_2O \rightarrow [Pd(H_2O)_4]^{+2}$$
$$\downarrow$$
$$Pd(OH)_2 + 2\ (H_3O)^+$$
$$\downarrow$$
$$\boxed{PdO} + H_2O$$
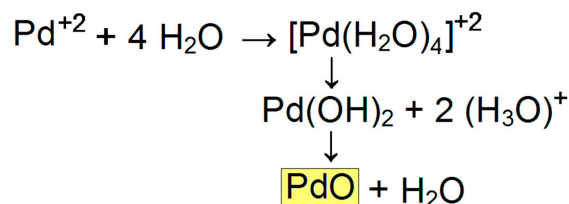
Scheme 1. Proposed mechanism of formation of palladium oxide nanoparticles.

In order to find a confirmation to this hypothesis and to understand the nature of the metal nanoparticles, we performed XRD, XPS and Raman measurements. By ultra-centrifuging a portion of the aqueous suspension, a dark deposit was obtained, rinsed with pure water and deposited on a silicon substrate for the XRD experiment (Figure 3) and on a glass substrate for both XPS (Figure 4) and micro-Raman measurements (Figure 5).
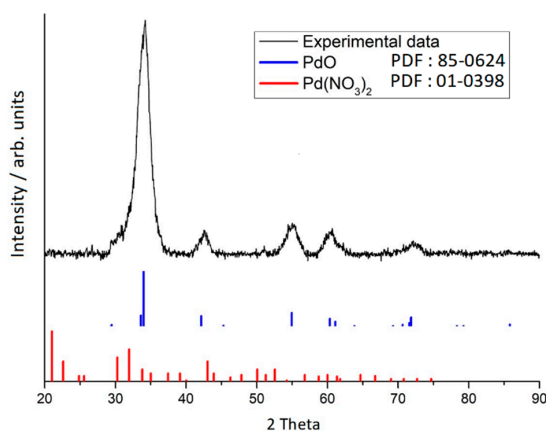

Figure 3. X-ray diffraction (XRD) of the centrifuged colloidal suspension, after drying on a silicon substrate. Reference diffraction patterns of palladium(II) oxide (PdO) (blue segments) and palladium(II) nitrate ($Pd(NO_3)_2$) (red segments) correspond to the Power Diffraction Files (PDF)s of palladium oxide and palladium nitrate, respectively.
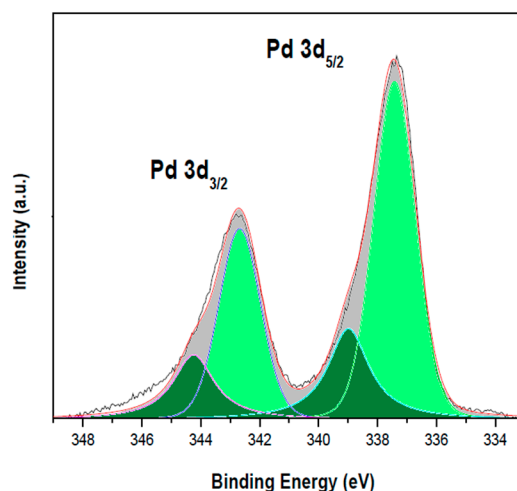
Figure 4. X-ray Photoelectron Spectroscopy (XPS) spectrum in the Pd 3*d* region, for colloidal nanoparticles deposited on glass. The predominant peaks, evidenced by light green color, correspond to Pd(II) oxide.
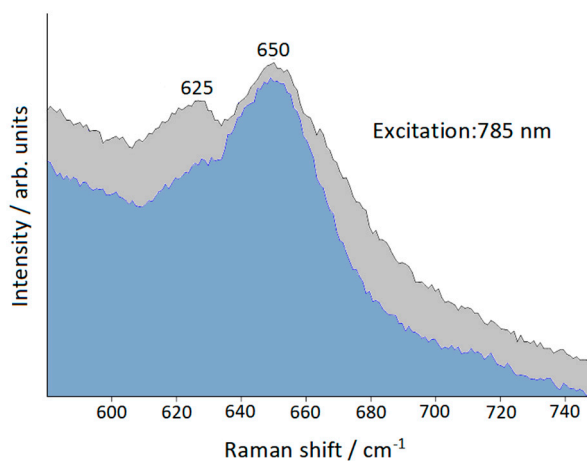

Figure 5. Micro-Raman spectra of deposited colloidal nanoparticles. The two spectra, evidenced by different colors, are representative of different points of the sample.

Figure 3 shows the experimental diffraction pattern (black line), along with the reference diffraction patterns of PdO (blue segments) and Pd(NO$_3$)$_2$ (red segments), corresponding to the Power Diffraction Files (PDF)s of the XRD database. By comparing the experimental pattern with the two reference patterns, it is possible to note that the experimental data are almost completely attributable to palladium oxide and just a small amount of palladium nitrate can be recognized. It is probably due to trace of the reactant solution. On the other side, a more thorough water cleaning is not recommended in order to avoid the alteration or aggregation of the nanoparticles. Moreover, the pronounced width of the peaks in the experimental diffraction pattern can be ascribable to the nature of the analyzed solid, as a secondary proof of the nanoparticle presence.

The XPS spectrum of the Pd 3*d* transition region is reported in Figure 4. Due to spin-orbit coupling, this transition results in two peaks: 3$d_{5/2}$ and 3$d_{3/2}$ at about 335 eV and 340 eV, respectively. Referring to the 3$d_{5/2}$ peak, it can be fit with two components: the first one predominant at 337.4 eV and the second one minority at 339.0 eV. The peak at 337.4 eV can be confidently attributed to PdO, according to our

previous investigations on palladium surfaces [42], even if an upshift is observed with respect to the value of 336.9 eV. This shift, generally shown by nanoparticles with respect to the bulk [43], can be explained on the basis of a quantic confinement. The other peak at 339.0 eV could be attributed to $Pd(OH)_2$, in analogy with that observed at 338.4 eV [42], or to a species of hydrate palladium oxide. Raman measurements, along with DFT calculations, can provide useful information in this regard.

Figure 5 shows two Raman spectra of the deposited colloidal nanoparticles, representative of different points of the sample, obtained with the micro-Raman apparatus. The intense band at 650 cm^{-1}, observed in both spectra, is attributable to PdO, according to the literature [44,45], whereas the shoulder around 625 cm^{-1}, with variable intensity depending on the irradiated points of the sample, could be attributed to the minority species observed in the XPS spectrum. This secondary band can be correctly assigned with the help of DFT calculations, which allow for collecting information on the species observed in the Raman spectra.

As shown in Figure 6, for the PdO molecule, a band at 649 cm^{-1} is predicted by the DFT calculations, fitting quite well with the Raman band observed at 650 cm^{-1}, whereas for $Pd(OH)_2$, the Raman band occurring at 625 cm^{-1} is not reproduced, because the symmetric and antisymmetric stretching modes of the Pd–O bonds are predicted at 567 and 517 cm^{-1}, respectively. Instead, considering palladium oxide coordinated to one water molecule, we calculated two bands at 625 and 647 cm^{-1}, which fit well with the bands observed in the Raman spectrum, which can be attributed to the PdO stretching mode mixed with the H bending mode of the water molecule. Figure 6 also shows the optimized structures of the species considered in the DFT calculations. The short hydrogen bond distance O – – – H–O–H (1.631 Å) in the PdO/H_2O complex, along with a significant negative charge-transfer from PdO to H_2O (−0.085 e), points to a form of palladium oxide strongly bound to water.

TABLE 1 – Calculated Raman frequencies (cm⁻¹)
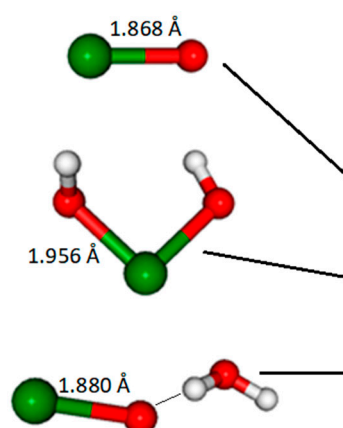
Molecule	Frequency	Assignment
PdO	649	Pd-O stretching
$Pd(OH)_2$	517 567	Pd-O stretching (antisymm.) Pd-O stretching (symm.)
PdO/H_2O	625 647	H bending + Pd-O stretching Pd-O stretching + H bending

Figure 6. Calculated Raman frequencies for the possible species present in the colloidal nanoparticles, whose optimized structures are shown.

Finally, we have evaluated the catalytic activity of our PdO nanoparticles by monitoring the reduction of *p*-nitrophenol (PNP) in borohydride solution, which is only possible in the presence of an appropriate catalyst [46] and represents a classical test for its efficiency [47–51]. By adding $NaBH_4$, the aqueous solution of PNP becomes alkaline and the absorption band of *p*-nitrophenolate occurs at 400 nm in the absorption spectrum, which does not appreciably decrease in time. When, instead, a small quantity of the colloidal suspension of PdO nanoparticle is added to the aqueous solution, the peak at 400 nm decreases exponentially, while the absorption peak of *p*-aminophenol grows around 300 nm, as shown in Figure 7. This evidence points to a catalytic reduction of PNP by the effect of the palladium oxide nanoparticles added to the aqueous solution.
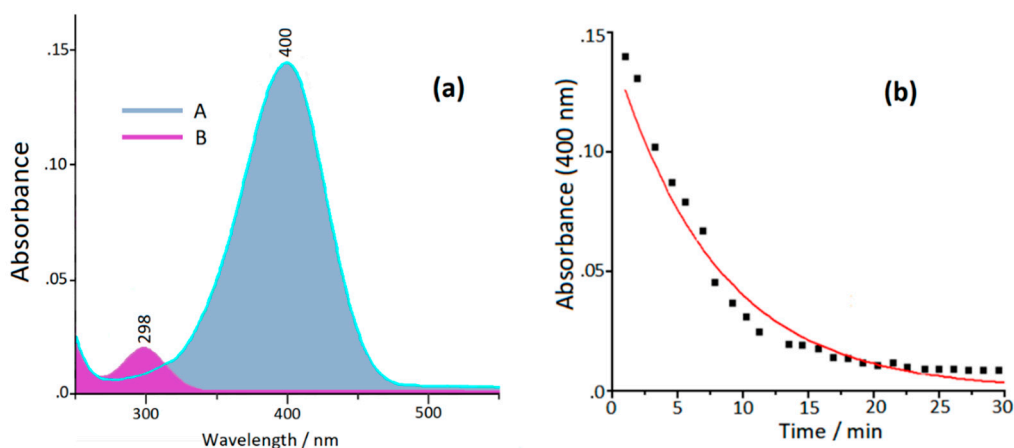
Figure 7. (**a**) UV-vis absorption spectra of the PNP/NaBH$_4$ solution before (A) and after 30 min (B) from the addition of the PdO colloidal sample [optical path length (OPL) = 1 cm]; (**b**) time evolution of the 400 nm extinction band.

4. Conclusions

We proposed a very simple method to obtain stable palladium oxide nanoparticles dispersed in water, without the aid of additional material, by dissolving palladium nitrate in water at a concentration around 10^{-4} M. TEM microscopy showed the presence of very small nanoparticles, mostly monodisperse, whose colloidal stability was also proven by zeta-potential measurements. The particle characterization, performed with different techniques, such as UV absorption, XRD diffraction, XPS and Raman spectroscopy, along with DFT calculations, allowed both to validate the mechanism of formation of the nanoparticles and to identify their chemical composition. The colloidal nanoparticles are mostly constituted by Pd(II) oxide, along with a minority species formed by PdO strongly coordinated to water. These nanoparticles showed a marked catalytic activity, evaluated by monitoring the reduction of *p*-nitrophenol to *p*-aminophenol. Hence, they can be usefully employed in processes of heterogeneous catalysis, in particular those concerning the catalytic degradation of aromatic derivatives that represent a serious danger for the environment as pollutants, as in the case of *p*-nitrophenol.

Author Contributions: M.M.-M., performed TEM, Raman and absorption measurements; N.C. recorded XPS and XRD measurements, A.Z. performed catalysis tests, F.M.-M. carried out DFT calculations; M.M.-M. coordinated the research. All authors have read and agreed to the published version of the manuscript.

References

1. Blazer, H.-U.; Indolese, A.; Schnyder, A.; Steiner, H.; Studer, M. Supported palladium catalysts for fine chemicals synthesis. *J. Mol. Catal. A Chem.* **2001**, *173*, 3–18. [CrossRef]
2. Liu, X.; Astruc, D. Development of the Applications of Palladium on Charcoal in Organic Synthesis. *Adv. Synth. Catal.* **2018**, *360*, 3426–3459. [CrossRef]
3. Astruc, D.; Lu, F.; Aranzaes, J.R. Nanoparticles as recyclable catalysts: The frontier between homogeneous and heterogeneous catalysis. *Angew. Chem. Int. Ed.* **2005**, *44*, 7852–7872. [CrossRef]
4. Grunes, J.; Zhu, A.; Somorjai, G.A. Catalysis and nanoscience. *Chem. Commun.* **2003**, 2257–2260. [CrossRef]
5. Nishihata, Y.; Mizuki, J.; Akao, T.; Tanaka, H.; Uenishi, M.; Kimura, M.; Okamoto, T.; Hamada, N. Self-regeneration of a Pd-perovskite catalyst for automotive emissions control. *Nature* **2002**, *418*, 164–167. [CrossRef] [PubMed]

6. Bräse, S.; Kirchhoff, J.H.; Köbberling, J. Palladium-catalyzed reaction in solid phase organic synthesis. *Tetrahedron* **2003**, *59*, 885–939.

7. Mei, Y.; Lu, Y.; Polzer, F.; Ballauff, M.; Drechsler, M. Catalytic activity of palladium nanoparticles encapsulated in spherical polyelectrolyte brushes and core-shell microgels. *Chem. Mater.* **2007**, *19*, 1062–1069. [CrossRef]

8. Jv, X.; Sun, S.; Zhang, Q.; Du, M.; Wang, L.; Wang, B. Efficient and Mild Reductive Amination of Carbonyl Compounds Catalyzed by Dual-Function Palladium Nanoparticles. *ACS Sustain. Chem. Eng.* **2020**, *8*, 1618–1626. [CrossRef]

9. Trzeciak, A.M.; Augustyniak, A.W. The role of palladium nanoparticles in catalytic C–C cross-coupling reactions. *Co-ord. Chem. Rev.* **2019**, *384*, 1–20. [CrossRef]

10. Bej, A.; Ghosh, K.; Sarkar, A.; Knight, D.W. Palladium nanoparticles in the catalysis of coupling reactions. *RSC Adv.* **2016**, *6*, 11446–11453. [CrossRef]

11. Favier, I.; Pla, D.; Gómez, M. Palladium Nanoparticles in Polyols: Synthesis, Catalytic Couplings, and Hydrogenations. *Chem. Rev.* **2020**, *120*, 1146–1183. [CrossRef] [PubMed]

12. Pérez-Lorenzo, M. Palladium Nanoparticles as Efficient Catalysts for Suzuki Cross-Coupling Reactions. *J. Phys. Chem. Lett.* **2012**, *3*, 167–174. [CrossRef]

13. Nasrollahzadeh, M.; Sajadi, S.M.; Maham, M. Green synthesis of palladium nanoparticles using Hippophae rhamnoides Linn leaf extract and their catalytic activity for the Suzuki–Miyaura coupling in water. *J. Mol. Catal. A Chem.* **2015**, *396*, 297–303. [CrossRef]

14. Kalaiselvi, A.; Mohana Roopan, S.; Madhumitha, G.; Ramalingam, C.; Elango, G. Synthesis and characterization of palladium nanoparticles using Catharanthus roseus leaf extract and its application in the photo-catalytic degradation. *Spectrochim. Acta A* **2015**, *135*, 116–119. [CrossRef]

15. Zhu, G.H.; Han, J.Y.; Zernlyanov, D.Y.; Ribeiro, F.H. Temperature dependence of the kinetics for the complete oxidation of methane on palladium and palladium oxide. *J. Phys. Chem. B* **2005**, *109*, 2331–2337. [CrossRef]

16. Oh, S.H.; Hoflund, G.B. Low-temperature catalytic carbon monoxide oxidation over hydrous and anhydrous palladium oxide powders. *J. Catal.* **2007**, *245*, 35–44. [CrossRef]

17. Lichtenberger, J.; Lee, D.; Iglesia, E. Catalytic oxidation of methanol on Pd metal and oxide clusters at near-ambient temperatures. *Phys. Chem. Chem. Phys.* **2007**, *9*, 4902–4906. [CrossRef]

18. Fujimoto, K.-I.; Ribeiro, F.H.; Avalos-Borja, M.; Iglesia, E. Structure and Reactivity of PdO_x/ZrO_2 Catalysts for Methane Oxidation at Low Temperatures. *J. Catal.* **1998**, *179*, 431–442. [CrossRef]

19. Wang, K.M.; Huang, T.; Liu, H.F.; Zhao, Y.X.; Liu, H.M.; Sun, C.T. Size control synthesis of palladium oxide nanoparticles by microwave irradiation. *Colloids Surf. A* **2008**, *325*, 21–25. [CrossRef]

20. Bagchi, V.; Bandyopadhyay, D. *In situ* generation of palladium oxide nano-crystals. *J. Organomet. Chem.* **2009**, *694*, 1259–1262. [CrossRef]

21. Meher, S.; Rana, R.K. A rational design of a Pd-based catalyst with a metal-metal oxide interface influencing molecular oxygen in the aerobic oxidation of alcohols. *Green Chem.* **2019**, *21*, 2494–2503. [CrossRef]

22. Wu, Q.; Rao, Z.; Yuan, L.; Jiang, L.; Sun, G.; Ruan, J.; Zhou, Z.; Sang, S. Carbon supported PdO with improved activity and stability for oxygen reduction reaction in alkaline solution. *Electrochim. Acta* **2014**, *150*, 157–166. [CrossRef]

23. Frisch, M.J.; Trucks, G.W.; Schlegel, H.B.; Scuseria, G.E.; Robb, M.A.; Cheeseman, J.R.; Scalmani, G.; Barone, V.; Petersson, G.A.; Nakatsuji, H.; et al. *Gaussian 09*; Revision, D.01; Gaussian, Inc.: Wallingford, CT, USA, 2009.

24. Lee, C.; Yang, W.; Parr, R.G. Development of the Colle-Salvetti correlation-energy formula into a functional of the electron density. *Phys. Rev. B* **1988**, *37*, 785–789. [CrossRef] [PubMed]

25. Becke, A.D. Density-functional thermochemistry. III. The role of exact exchange. *J. Chem. Phys.* **1993**, *98*, 5648–5652. [CrossRef]

26. Hay, P.J.; Wadt, W.R. Ab initio effective core potentials for molecular calculations. Potentials for the transition metal atoms Sc to Hg. *J. Chem. Phys.* **1985**, *82*, 270–283. [CrossRef]

27. Wadt, W.R.; Hay, P.J. Ab initio effective core potentials for molecular calculations. Potentials for main group elements Na to Bi. *J. Chem. Phys.* **1985**, *82*, 284–298. [CrossRef]

28. Hay, P.J.; Wadt, W.R. Ab initio effective core potentials for molecular calculations. Potentials for K to Au including the outermost core orbitals. *J. Chem. Phys.* **1985**, *82*, 299–310. [CrossRef]

29. Gellini, C.; Deepak, F.L.; Muniz-Miranda, M.; Caporali, S.; Muniz-Miranda, F.; Pedone, A.; Innocenti, C.; Sangregorio, C. Magneto-plasmonic colloidal nanoparticles obtained by laser ablation of nickel and silver targets in water. *J. Phys. Chem. C* **2017**, *121*, 3597–3606. [CrossRef]

30. Zoppi, A.; Caporali, S.; Muniz-Miranda, F.; Pedone, A.; Muniz-Miranda, M. Adsorption of Trans-Zeatin on Laser-Ablated Gold Nanoparticles for Transport into Plant Cells and Growth Stimulation. *ACS Appl. Nano Mater.* **2019**, *2*, 7319–7327. [CrossRef]

31. López-Tocón, I.; Valdivia, S.; Soto, J.; Otero, J.C.; Muniz-Miranda, F.; Menziani, M.C.; Muniz-Miranda, M. A DFT Approach to the Surface-Enhanced Raman Scattering of 4-Cyanopyridine Adsorbed on Silver Nanoparticles. *Nanomaterials* **2019**, *9*, 1211. [CrossRef]

32. Muniz-Miranda, M.; Pagliai, M.; Muniz-Miranda, F.; Schettino, V. Raman and computational study of solvation and chemisorption of thiazole in silver hydrosol. *Chem. Commun.* **2011**, *47*, 3138–3140. [CrossRef] [PubMed]

33. Pagliai, M.; Muniz-Miranda, F.; Schettino, V.; Muniz-Miranda, M. Competitive Solvation and Chemisorption in Silver Colloidal Suspensions. *Prog. Colloid Polym. Sci.* **2012**, *139*, 39–44.

34. Muniz-Miranda, M.; Muniz-Miranda, F.; Caporali, S. SERS and DFT study of copper surfaces coated with corrosion inhibitor. *Beilstein J. Nanotechnol.* **2014**, *5*, 2489–2497. [CrossRef] [PubMed]

35. Muniz-Miranda, F.; Pedone, A.; Muniz-Miranda, M. Spectroscopic and DFT investigation on the photo-chemical properties of a push-pull chromophore: 4-Dimethylamino-4′-nitrostilbene. *Spectrochim. Acta A* **2018**, *190*, 33–39. [CrossRef] [PubMed]

36. Gellini, C.; Muniz-Miranda, F.; Pedone, A.; Muniz-Miranda, M. SERS active Ag-SiO$_2$ nanoparticles obtained by laser ablation of silver in colloidal silica. *Beilstein J. Nanotechnol.* **2018**, *9*, 2396–2404. [CrossRef]

37. Pestryakov, A.N.; Lunin, V.V.; Fuentes, S.; Bogdanchikova, N.; Barrera, A. Influence of modifying additives on the electronic state of supported palladium. *Chem. Phys. Lett.* **2003**, *367*, 102–108. [CrossRef]

38. Kravchuk, L.S.; Stel'mak, E.I.; Ivashchenko, N.I.; Valieva, S.V.; Molod'yanova, V.S. Formation and physicochemical properties of the system palladium oxide (PdO)/ZrO$_2$. *Kinetika i Kataliz* **1992**, *33*, 672–677.

39. Martínez, J.M.; Torrico, F.; Pappalardo, R.R.; Sánchez Marcos, E. Understanding the Hydration Structure of Square-Planar Aquaions: The [Pd(H$_2$O)$_4$]$^{2+}$ Case. *J. Phys. Chem. B* **2004**, *108*, 15851–15855. [CrossRef]

40. Adnan Ali Shah, S.; Hofer, T.S.; Qaiser Fatmi, M.; Randolf, B.R.; Rode, B.M. A QM/MM MD simulation study of hydrated Pd^{2+}. *Chem. Phys. Lett.* **2006**, *426*, 301–305. [CrossRef]

41. Torrico, F.; Pappalardo, R.R.; Sánchez Marcos, E.; Martínez, J.M. Hydration Structure and Dynamic Properties of the Square Planar Pt(II) Aquaion Compared to the Pd(II) Case. *Theor. Chem. Accounts* **2006**, *115*, 196–203. [CrossRef]

42. Muniz-Miranda, M.; Muniz-Miranda, F.; Caporali, S.; Calisi, N.; Pedone, A. SERS, XPS and DFT investigation on palladium surfaces coated with 2, 2′-bipyridine monolayers. *Appl. Surf. Sci.* **2018**, *457*, 98–103. [CrossRef]

43. Jürgensen, A.; Heutz, N.; Raschke, H.; Merz, K.; Hergenröder, R. Behavior of Supported Palladium Oxide Nanoparticles under Reaction Conditions, Studied with near Ambient Pressure XPS. *Anal. Chem.* **2015**, *87*, 7848–7856. [CrossRef] [PubMed]

44. Remillard, J.T. Optical studies of PdO thin films. *J. Appl. Phys.* **1992**, *71*, 4515–4522. [CrossRef]

45. Weber, W.H.; Baird, R.J.; Graham, G.W. Raman Investigation of Palladium Oxide, Rhodium Sesquioxide and Palladium Rhodium Dioxide. *J. Raman Spectrosc.* **1988**, *19*, 239–244. [CrossRef]

46. Pozun, Z.D.; Rodenbusch, S.E.; Keller, E.; Tran, K.; Tang, W.; Stevenson, K.J.; Henkelman, G. A Systematic Investigation of *p*-Nitrophenol Reduction by Bimetallic Dendrimer Encapsulated Nanoparticles. *J. Phys. Chem. C* **2013**, *117*, 7598–7604. [CrossRef]

47. Krishna, R.; Fernandes, D.M.; Dias, C.; Ventura, J.; Venkata Ramana, E.; Freire, C.; Titus, E. Novel synthesis of Ag@Co/RGO nanocomposite and its high catalytic activity towards hydrogenation of 4-nitrophenol to 4-aminophenol. *Int. J. Hydrogen Energy* **2015**, *40*, 4996–5005. [CrossRef]

48. Rocha, M.; Fernandes, C.; Pereira, C.; Rebelo, S.L.H.; Pereira, M.F.R.; Freire, C. Gold-supported magnetically recyclable nanocatalysts: A sustainable solution for the reduction of 4-nitrophenol in water. *RSC Adv.* **2015**, *5*, 5131–5141. [CrossRef]

49. Ayán-Varela, M.; Fernández-Merino, M.J.; Paredes, J.I.; Villar-Rodil, S.; Fernández-Sánchez, C.; Guardia, L.; Martínez-Alonso, A.; Tascón, J.M.D. Highly efficient silver-assisted reduction of graphene oxide dispersions at room temperature: Mechanism, and catalytic and electrochemical performance of the resulting hybrids. *J. Mater. Chem. A* **2014**, *2*, 7295–7305. [CrossRef]

50. Barman, B.K.; Nanda, K.K. Rapid reduction of GO by hydrogen spill-over mechanism by in situ generated nanoparticles at room temperature and their catalytic performance towards 4-nitrophenol reduction and ethanol oxidation. *Appl. Catal. A Gen.* **2015**, *491*, 45–51. [CrossRef]

51. Ren, R.; Li, S.; Li, J.; Ma, J.; Liu, H.; Ma, J. Enhanced catalytic activity of Au nanoparticles self-assembled on thiophenol functionalized graphene. *Catal. Sci. Technol.* **2015**, *5*, 2149–2156. [CrossRef]